Intelligent adaptive model of helicopter turboshaft engines gas temperature sensor thermocouple

Serhii Vladov[1,*,†], Nataliia Vladova[2,†], Victoria Vysotska[3,†], Vasyl Lytvyn[3,†], Mykhailo Luchkevych[3,†]and Kateryna Surkova[2,†]

[1] *Kharkiv National University of Internal Affairs, L. Landau Avenue 27 61080 Kharkiv, Ukraine*

[2] *Ukrainian State Flight Academy, Chobanu Stepana Street 1 25005 Kropyvnytskyi, Ukraine*

[3] *Information Systems and Networks Department, Lviv Polytechnic National University, Stepan Bandera Street 12 79013 Lviv, Ukraine*

Abstract

The paper presents a model for the helicopter turboshaft engine gas temperature sensor thermocouple dynamics modeling based on a heat transfer physical model combination, a recurrent LSTM neural network with an attention mechanism, and an adaptive Kalman filter. The thermocouple discrete model is obtained that takes into account the heat capacity and thermal resistance, using the expansion of a nonlinear dependence in the operating point vicinity through a Taylor series. A modified LSTM architecture is developed that accepts engine parameters as input, transformed through an attention mechanism to extract relevant features. The neural network output is corrected by an adaptive Kalman filter, which is able to adjust the noise variance at each step and also suppresses out-of-band signal components using a bandpass filter. A computational experiment showed that the reconstructed temperature in front of the compressor turbine curve accurately reproduces the reference signal: the values do not deviate by more than 2...3 K, and the absolute error is kept within ± 1 K in the vast majority of points. To evaluate the training characteristics, two integral indicators were used: the efficiency coefficient K_{eff} and the quality coefficient $K_{quality}$, which, in comparison with classical LSTM, GRU, and RNN, showed the adaptability and convergence best balance (K_{eff} up to 0.991, $K_{quality}$ up to 0.989). Additional analysis on the accuracy, precision, recall, and F1-score metrics confirmed the model's superiority (up to 0.993, 0.988, 0.986, and 0.987, respectively).

Keywords

LSTM network, attention mechanism, adaptive Kalman filter, dynamic modeling, gas temperature sensor thermocouple, helicopter turboshaft engine

1. Introduction

In modern helicopter turboshaft engines (TE), accurate gas temperature measurement is a key factor in ensuring optimal operation, reducing component wear, and increasing overall flight safety [1–3]. Thermocouples have traditionally been used as the main sensing element [4, 5] for such measurements, but with rapid load changes and pressure fluctuations, classical signal processing algorithms [6, 7] exhibit significant delays and errors. This is especially critical in helicopter flight conditions [8, 9], where the speed and accuracy of the engine control systems efficiency and overheating protection data are directly affected.

The research relevance is due to increased requirements for aviation equipment efficiency and environmental friendliness, as well as the need for helicopter resource capabilities to expand in severe and changeable weather conditions [10]. The intelligent adaptive thermocouple model's use will reduce the risk of thermal damage to turbine blades, optimize fuel consumption, and reduce

*MoDaST 2025: Modern Data Science Technologies Doctoral Consortium, June, 15, 2025, Lviv, Ukraine

[1,*] Corresponding author.

[†] These authors contributed equally.

serhii.vladov@univd.edu.ua (S. Vladov); nataliia.vladova@sfa.org.ua (N. Vladova); victoria.a.vysotska@lpnu.ua (V. Vysotska); vasyl.v.lytvyn@lpnu.ua (V. Lytvyn); mykhailo.m.luchkevych@lpnu.ua (M. Luchkevych); eskirua@sfa.org.ua (K. Surkova)

0000-0001-8009-5254 (S. Vladov); 0009-0009-7957-7497 (N. Vladova); 0000-0001-6417-3689 (V. Vysotska); 0000-0002-9676-0180 (V. Lytvyn); 0000-0002-2196-252X (M. Luchkevych); 0000-0002-1388-7611 (K. Surkova)

accidents associated with the temperature conditions incorrect diagnostics. The intelligent adaptive thermocouple model integration into on-board monitoring systems creates the prerequisites for the predictive maintenance development and the operating helicopter TE process further automation [11, 12].

In this research, an intelligent adaptive thermocouple model is built on modern machine learning methods [13, 14] and digital filtering [15, 16], which allows the temperature estimation parameters automatic adjustment in real time. Due to self-adjustment to the gas flow current dynamic characteristics, including pressure pulsations, variations in fuel composition, and temperature gradients in the channel [17], the developed model can significantly reduce constant and dynamic measurement errors. As a result, the response speed during transient engine operation modes increases, and the thermal state control system improves stability.

2. Related works

Modern research in the helicopter TE gas temperature parameters measuring field emphasizes the data coming from thermocouples accuracy and critical importance [4, 5, 10]. Under the pressure pulsations, vibrations, and high temperatures influence, traditional signal processing methods, such as uncontrolled noise filtering [15, 16, 18] or static calibration tables [6, 7], demonstrate significant errors and delays in response time. The elimination of these errors is relevant in transient engine operating modes, when timely adjustments are important to prevent overheating and component wear.

Machine learning methods, in particular neural networks [19–23] and Kalman filters [24–27], are increasingly used to improve the measurements accuracy and efficiency. Thus, in [19], a multilayer neural network with a closed dynamic compensation loop was proposed, which, after 280 training epochs, achieved a 99.5% accuracy when integrating thermocouple signals, significantly surpassing classical median-recursive [28] and recursive filters [29] in the first and second kinds of reducing errors. Similarly, the radial-basis neural networks used in combination with a multidimensional Kalman filter made it possible to ensure the accuracy of the identifying helicopter TE parameters at a 99.75% level [24].

Along with neural networks, hybrid approaches to digital filtering are also being developed [30–32]. Adaptive filters based on classical median and averaging algorithms, in combination with digital filtering algorithms with a variable sliding window function, demonstrate better noise suppression characteristics without significant dynamic response loss [33]. However, their efficiency decreases with strong nonlinearities and sharp transient processes under conditions that stimulate the search for new filtering structures and self-tuning algorithms in real time.

Despite the successes achieved, there are still unanswered questions that require further development of intelligent adaptive models. Balancing the onboard computers computing resources and the model complexity remains a problem, since many methods require GPU acceleration, which is not available in aircraft controllers. At the same time, the algorithm's stability in extreme weather conditions and sensor degradation in the field has not been tested extensively enough. Also, preventing issues of overfitting with limited training datasets and ensuring the model's ability to train online on flying platforms are open.

Thus, there is an urgent need to develop an intelligent adaptive thermocouple model that would combine deep learning methods (e.g., recurrent neural networks with attention mechanisms) and digital filters (adaptive Kalman filter with frequency domain filtering), taking into account the avionics real limitations. The developed model should provide dynamic compensation and self-tuning for changing engine operating modes, minimize response delays, and maintain high measurement accuracy even with insufficient training data and limited processing resources.

3. Materials and methods

3.1. The thermocouple dynamic model development

Based on [4, 5], the thermocouple is modeled as a single-circuit heat-capacitive element with thermal capacitance C and thermal resistance R relative to the gas as:

$$C \cdot \frac{dT_C(t)}{dt} + \frac{T_C(t) - T_G(t)}{R} = 0, \tag{1}$$

where $T_C(t)$ is the thermocouple junction temperature, T_G is the helicopter TE gas in front of the turbine compressor true value.

For the explicit Euler scheme further application (1) is rewritten as:

$$\frac{dT_C(t)}{dt} = \frac{1}{\tau} \cdot \left(T_C(t) - T_G(t)\right), \tag{2}$$

where $\tau = C \cdot R$.

Discretization (2) with a step Δt using the explicit Euler scheme has the form:

$$T_C[k+1] = T_C[k] + \Delta t \cdot \left(\frac{-1}{\tau} \cdot \left(T_C[k] - T_G[k]\right)\right). \tag{3}$$

To account for small temperature deviations around the operating point T_0, when high accuracy does not require taking into account all higher orders of nonlinearity, the T_C dependence local approximation using a polynomial is used. Assuming that $f(T_C) = \exp(-a \cdot T_C)$, for an arbitrary smooth function $f(T_C)$ around the operating point T_0, its Taylor series consists of the following components:

$$f\left(T_C\right) = \sum_{n=0}^{\infty} \frac{f^{(n)}\left(T_0\right)}{n!} \cdot \left(T_C - T_0\right)^n = f\left(T_0\right) + f'\left(T_0\right) \cdot \Delta T + \frac{f''\left(T_0\right)}{2!} \cdot (\Delta T)^2 + \frac{f'''\left(T_0\right)}{3!} \cdot (\Delta T)^3 + \ldots, \tag{4}$$

where $\Delta T = T_C - T_0$.

In (4), the zero-order term $a_0 = f(T_0)$ is a constant "offset" component that sets the baseline response level of the thermocouple. The first-order linear term $a_1 \cdot \Delta T = f'(T_0) \cdot (T_C - T_0)$ gives a proportional dependence of the output signal on the temperature deviation, which characterizes the sensor sensitivity. The second-order quadratic term $a_2 \cdot (\Delta T)^2 = \frac{f''\left(T_0\right)}{2!} \cdot \left(T_C - T_0\right)^2$ reflects the response curvature, since a large $|\Delta T|$ value this term begins to introduce corrections that are asymmetric in magnitude, affecting distortions during rapid temperature changes. Higher order terms ($n \geq 3$) $a_n \cdot (\Delta T)^n = \frac{f''\left(T_0\right)}{n!} \cdot \left(T_C - T_0\right)^n$ with each increase in n their contribution at small ΔT decreases as $O(\Delta T^n)$, but can become significant under extreme conditions. The remainder term estimation (Lagrange form) allows us to strictly estimate how much we are mistaken by truncating the series to the N-th order:

$$R_N = \frac{f^{(N+1)}(\xi)}{(N+1)!} \cdot \Delta T^{N+1}, \xi \in \left(T_0, T_C\right). \tag{5}$$

Denoting the increment as $\Delta T = T_C - T_0$ and the series coefficients as $a_1 = f'(T_0)$, $a_2 = \frac{f''(T_0)}{2!}$, $a_3 = \frac{f'''(T_0)}{3!}$,... the linear term contribution to the total change $f(T_C) - f(T_0)$ is equal to $a_1 \cdot \Delta T$, and this approximation "quality" is estimated by the relative contribution as:

$$\eta_1 = \frac{|a_1 \cdot \Delta T|}{\sum_{n=1}^{\infty} |a_n \cdot \Delta T^n|} \approx \frac{|a_1 \cdot \Delta T|}{|a_1 \cdot \Delta T| + |a_2 \cdot \Delta T^2|} = \frac{|f'(T_0) \cdot \Delta T|}{|f'(T_0) \cdot \Delta T| + \left|\frac{f''(T_0)}{2!} \cdot (\Delta T)^2\right|}. \quad (6)$$

For small ΔT the second approximation gives

$$\eta_1 \approx \frac{1}{1 + \left|\frac{f''(T_0)}{2 \cdot f'(T_0)}\right| \cdot \Delta T}, \quad (7)$$

which clearly shows how the linear term relative "strength" decreases with increasing $|\Delta T|$ and the second derivative.

Similarly, taking $a_1 = f'(T_0)$, $a_2 = \frac{f''(T_0)}{2!}$, $a_3 = \frac{f'''(T_0)}{3!}$,..., the quadratic term contribution to the total change $f(T_C) - f(T_0)$ is equal to $a_2 \cdot \Delta T^2$, and its relative "strength" is estimated as the first two terms sum fraction:

$$\eta_2 = \frac{|a_2 \cdot \Delta T^2|}{\sum_{n=1}^{\infty} |a_n \cdot \Delta T^n|} \approx \frac{|a_2 \cdot \Delta T^2|}{|a_1 \cdot \Delta T| + |a_2 \cdot \Delta T^2|} = \frac{\left|\frac{f''(T_0)}{2}\right| \cdot |\Delta T|^2}{|f'(T_0) \cdot \Delta T| + \left|\frac{f''(T_0)}{2}\right| \cdot |\Delta T|^2} = \frac{1}{\frac{2 \cdot |f'(T_0)|}{|f''(T_0)| \cdot |\Delta T|} + 1}. \quad (8)$$

From (8) it can be seen that when

$$|\Delta T| \gg \frac{2 \cdot |f'(T_0)|}{|f''(T_0)|} \quad (9)$$

the quadratic term begins to dominate ($\eta_2 \to 1$), and for small $|\Delta T|$ its influence is negligible ($\eta_2 \to 0$).

For $n \geq 3$, the contribution of each n-th term $a_n \cdot \Delta T^n = \frac{f^{(n)}(T_0)}{n!} \cdot (T_C - T_0)^n$ to the total change Δf can be estimated through this term relative "strength" as:

$$\eta_n = \frac{|a_n \cdot \Delta T^n|}{\sum_{m=1}^{\infty} |a_m \cdot \Delta T^m|} \approx \frac{\left|\frac{f^{(n)}(T_0)}{n!}\right| \cdot |\Delta T|^n}{\sum_{m=1}^{\infty} \left|\frac{f^{(m)}(T_0)}{m!}\right| \cdot |\Delta T|^m}, \quad (10)$$

where $N \geq n$. For the $|\Delta T|$ small values, the first (linear) and second (quadratic) terms will be the main ones, and for $n \geq 3$, $\eta_n = O(|\Delta T|^{n-1})$ order their relative contribution decreases rapidly.

For the remainder term rigorous estimate after truncating the series to order N, using the Lagrange form (5), an upper estimate is obtained in the form:

$$|R_N| \leq \frac{\max\limits_{u \in [T_0, T_C]} f^{(N+1)}(u)}{(N+1)!} \cdot |\Delta T|^{n+1}. \quad (11)$$

From (11) it is clear that for $|\Delta T| < 1$ the R_N value and all higher terms decrease as $O(|\Delta T|^{n+1})$, and it is sufficient to take $N = 2$ or $N = 3$ to ensure the given accuracy.

Thus, when expanding the thermocouple response function in a Taylor series, the zeroth order $n = 0$ specifies a constant "biased" component, the first order $n = 1$ ensures proportional (linear) following of the output signal to the temperature deviation, the second order $n = 2$ introduces a correction for the response curvature and thus takes into account average nonlinear effects, and the higher-order terms $n \geq 3$ describe more subtle, high-order nonlinearities, significant mainly for extreme variations in ΔT. In practice, for the helicopter TE gas temperature range, it is usually sufficient to truncate the series at $n = 2$ or $n = 3$, since the remainder term R_N becomes negligibly small.

3.2. Development of a recurrent neural network with attention mechanisms and a Kalman filter

It is assumed that at each k-th step the vector acts at the neural network input:

$$x_k = \left[T_C[k], u_k\right], \tag{12}$$

where u_k are additional parameters (flow rate, pressure, etc. [34]).

In this research, the developed recurrent neural network with attention mechanisms and a Kalman filter basis is the LSTM network (Figure 1), whose use is justified by the high accuracy (99% and higher) in solving applied problems of monitoring helicopter TE [19, 25, 35].

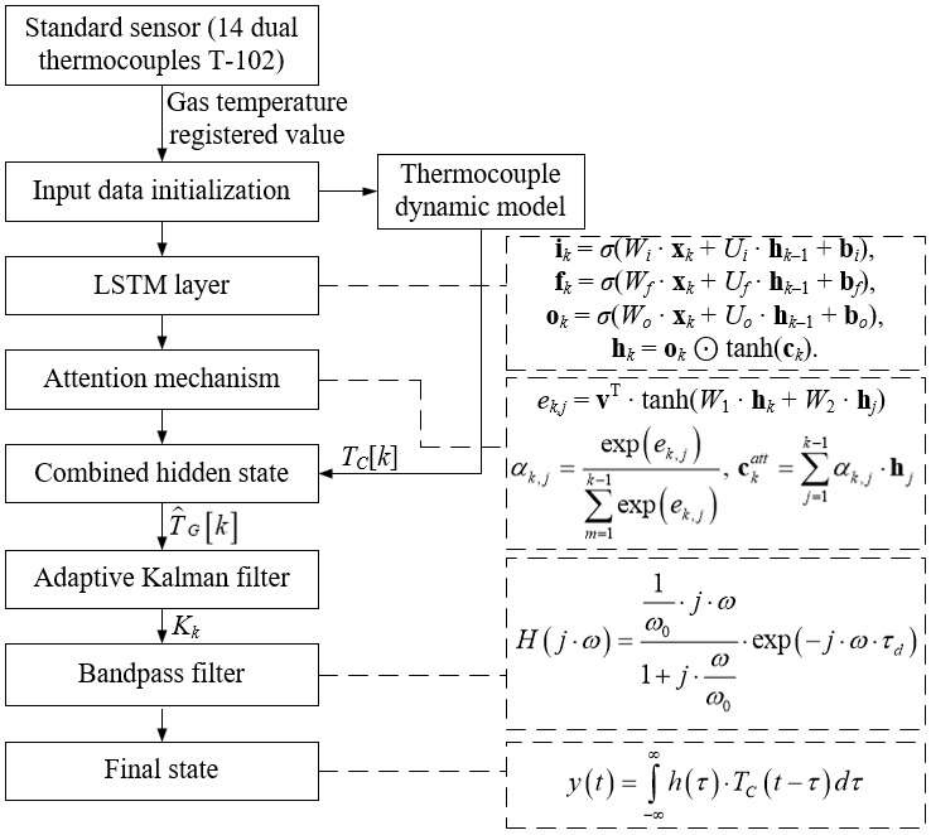

Figure 1: The developed model structural diagram with LSTM network, attention mechanism and adaptive Kalman filter. (author's development).

It is assumed that $h_k \in R^n$ is a hidden state, c_k is the LSTM network cell state. Then:

$$\begin{gathered} i_k = \sigma\left(W_i \cdot x_k + U_i \cdot h_{k-1} + b_i\right),\ f_k = \sigma\left(W_f \cdot x_k + U_f \cdot h_{k-1} + b_f\right),\ o_k = \sigma\left(W_o \cdot x_k + U_o \cdot h_{k-1} + b_o\right), \\ \tilde{c}_k = \tanh\left(W_c \cdot x_k + U_c \cdot h_{k-1} + b_c\right),\ c_k = f_k \odot c_{k-1} + i_k \odot \tilde{c}_k,\ h_k = o_k \odot \tanh\left(c_k\right). \end{gathered} \tag{13}$$

To focus on the most "important" past states $\{\mathbf{h}_1, \ldots, \mathbf{h}_{k-1}\}$, an attention mechanism is introduced, presented in the context:

$$e_{k,j}=v^T\cdot\tanh\left(W_1\cdot h_k+W_2\cdot h_j\right),\ \alpha_{k,j}=\frac{\exp\left(e_{k,j}\right)}{\sum_{m=1}^{k-1}\exp\left(e_{k,j}\right)},\ c_k^{att}=\sum_{j=1}^{k-1}\alpha_{k,j}\cdot h_j. \tag{14}$$

Then the "enriched" hidden state is defined as:

$$\tilde{h}_k=\tanh\left(W_h\left[h_k;c_k^{att}\right]\right). \tag{15}$$

Taking into account the above, the gas temperature prediction is determined as:

$$\hat{T}_G[k]=\omega_o^T\cdot\tilde{h}_k+b_o. \tag{16}$$

The adaptive Kalman filter combines the neural network output and the thermocouple dynamic model in the linear state system form $s_k=\left[T_C[k],\dot{T}_C[k]\right]^T$ and measurements $z_k=\hat{T}_G[k]$, which allows the temperature estimate recursive prediction and correction. Then the prediction is carried out according to the expression:

$$s_{k|k-1}=F\cdot s_{k-1|k-1},\ P_{k|k-1}=F\cdot P_{k-1|k-1}\cdot F^T+Q_k, \tag{17}$$

where $F=\begin{pmatrix}1 & \Delta t\\ 0 & 1-\frac{\Delta t}{\tau}\end{pmatrix}$, and the correction is according to the expression:

$$\begin{gathered}K_k=P_{k|k-1}\cdot H^T\cdot\left(H\cdot P_{k|k-1}\cdot H^T+R_k\right)^{-1},\ s_{k|k}=s_{k-1|k-1}+K_k\cdot\left(z_k-H\cdot s_{k|k-1}\right),\\ P_{k|k}=\left(I-K_k\cdot H\right)\cdot P_{k|k-1},\ H=\begin{bmatrix}1 & 0\end{bmatrix},\end{gathered} \tag{18}$$

where R_k is the measurement noise estimate, adaptively adjusted, according to the residuals recurrent estimate:

$$R_k=\lambda\cdot R_{k-1}+\left(1-\lambda\right)\cdot\left(z_k-H\cdot s_{k|k-1}\right)^2, \tag{19}$$

where $0 < \lambda < 1$.

Taking into account the helicopter avionics limitations (passing low-frequency thermal oscillations, damping high-frequency noise), to isolate in the thermocouple signal the frequency range corresponding to the gas temperature change actual dynamics (from ω_1 to ω_2), and to suppress noise components outside this interval, a bandpass filter is used, whose transfer function is described by the expression:

$$H\left(j\cdot\omega\right)=\frac{\frac{1}{\omega_0}\cdot j\cdot\omega}{1+j\cdot\frac{\omega}{\omega_0}}\cdot\exp\left(-j\cdot\omega\cdot\tau_d\right), \tag{20}$$

where ω_0 is the cutoff frequency (~ 0.1...10 Hz depending on the gas dynamics), τ_d is the signal transmission delay.

In the time domain, convolution is described by the expression:

$$y(t)=\int_{-\infty}^{\infty}h(\tau)\cdot T_C(t-\tau)\,d\tau. \tag{21}$$

Thus, the developed neural network with an attention mechanism and an adaptive Kalman filter (see Figure 1) is trained in real time [36], minimizing the total functional:

$$L=\sum_k\left(\tilde{T}_G[k]-T_G^{true}[k]\right)^2+\gamma\cdot\sum_k\left\|K_k-K_{k-1}\right\|^2, \tag{22}$$

with a regularizer for smooth changes in Kalman coefficients.

Backpropagation takes a step along the gradient [36, 37]:

$$\theta \leftarrow \theta - \eta \cdot \frac{\partial L}{\partial \theta}, \frac{\partial L}{\partial \theta} = \sum_k 2 \cdot \left(\widetilde{T}_G[k] - T_G[k] \right) \cdot \frac{\partial \widetilde{T}_G[k]}{\partial \theta} + 2 \cdot \gamma \cdot \left(K_k - K_{k-1} \right) \cdot \frac{\partial K_k}{\partial \theta}. \quad (23)$$

In practical implementation, all parameters (W_i, U_i, b_i, τ, ω_0, adaptive covariances Q_k, R_k, etc.) are selected based on historical data of experimental changes in helicopter TE parameters.

3.3. The developed model software implementation

The developed model is implemented in the Matlab Simulink R2014b software environment (Figure 2), where the input signal $T_C[k]$ and the additional parameters u_k vector are fed to the subsystem "Thermocouple dynamic model," implemented by the MATLAB Function block with the equation $T_C[k+1] = T_C[k] + \Delta t \cdot \left(\frac{-1}{\tau} \cdot \left(T_C[k] - T_G[k] \right) \right)$. Normalized data in the sequence form are fed to the LSTM cell implemented by the MATLAB Function block with the corresponding equations (13), and then to the attention mechanism, also implemented by the MATLAB Function block with equation (14), which forms a $\hat{T}_G[k]$ estimate according to (16). The obtained estimate, together with the state vector $s_k = \left[T_C[k], \dot{T}_C[k] \right]^T$ is fed to the Adaptive Kalman Filter subsystem, implemented as a series-connected Discrete State-Space, MATLAB Function, and Kalman Filter blocks, which outputs the purified value $\overline{T}_G[k]$. Then the signal $\overline{T}_G[k]$ is filtered by frequency content through the Digital Filter Design and BandPass Filter blocks, and the final signal $T_{out}[k]$ is output to Scope.

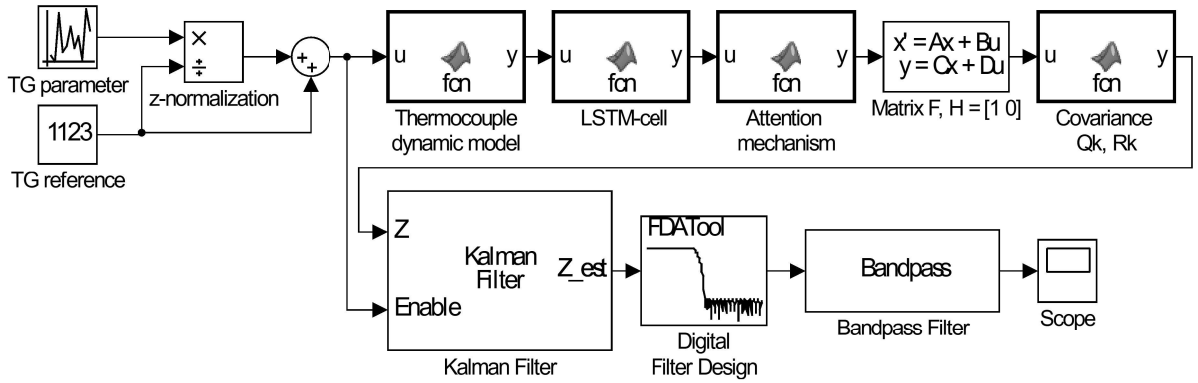

Figure 2: The developed model scheme software implementation in the Matlab Simulink R2014b software environment. (author's development).

4. Case study

4.1. The initial data analysis and pre-processing

In the computational experiment for the helicopter TE's thermal dynamics modeling in the nominal operating mode, the TV3-117 engine [8, 9, 11, 19, 24, 35, 36] gas temperature in front of the compressor turbine $T_G(t)$ real measurement number was used. The measurements were carried out on board the serial Mi-8MTV helicopter using a standard sensor, which is a set of 14 dual chrome-alumel thermocouples of the T-102 type [8, 9, 11, 19, 24, 35, 36]. The tests were carried out at a 2500-meter altitude above sea level under standard atmospheric conditions (air temperature ≈ 268 K, pressure ≈ 74 kPa). The signals were recorded with a Δt = 0.25 seconds periodicity (sampling frequency 4 Hz) for 320 seconds, which yielded 1280 readings in the final sample. The thermocouple signals were preprocessed by the onboard controller. A two-stage algorithm was used to filter out noise: smoothing with a sliding window of average length 11 readings (Savitzky–Golay, third-order polynomial [38]) and removing outliers according to the "±3σ" principle, followed by the gaps linear interpolation. When correcting for systematic errors, the thermocouples calibration characteristic (error ≤ 1.5 K) and a correction for flow velocity (up to 20

m/s) were taken into account. After cleaning and checking for homogeneity (Shapiro–Wilk and Durbin–Watson [39] tests), the time series was reduced to a single scale using classical *z*-normalization:

$$z\left(T_G\right)_i = \frac{T_{G_{meas}}^{(i)} - \frac{1}{N}\cdot\sum_{i=1}^{N} T_{G_{meas}}^{(i)}}{\frac{1}{N}\cdot\sum_{i=1}^{N}\left(T_{G_{meas}}^{(i)} - \frac{1}{N}\cdot\sum_{i=1}^{N} T_{G_{meas}}^{(i)}\right)^2}, \tag{24}$$

where $N = 4 \cdot 320 = 1280$.

According to the data in Figure 3, the gas temperature in front of the turbine maximum absolute temperature reached 1140 K in the exposure approximately 130...160 seconds interval; after that, a smooth decline to 1090 K is observed by the record end. The resulting normalized series $z(t)$ was then used in adaptive algorithms for estimating the heat transfer model and for constructing correlation function parameters with the engine output parameters.

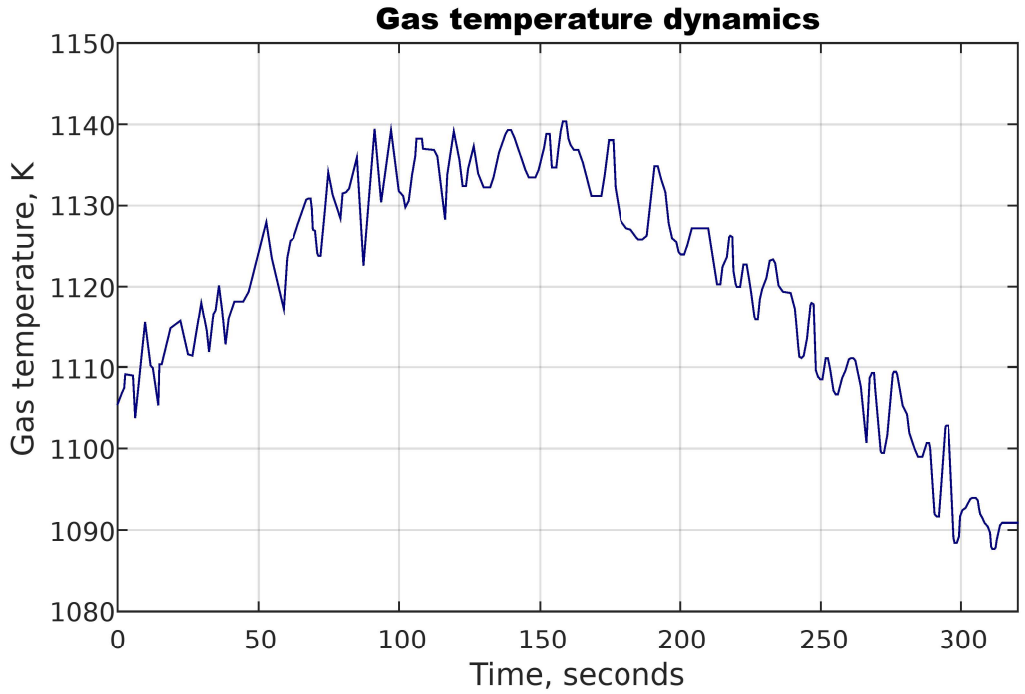

Figure 3: The gas temperature in front of the compressor turbine initial signal diagram, recorded on board the helicopter by a standard sensor. (author's development).

To form the training dataset, the gas temperature in front of the compressor turbine normalized values were used. This dataset fragment is presented in Table 1. The tests conducted confirmed that the dataset complies with the Fisher-Pearson [40, 41] and Fisher-Snedecor [42, 43] homogeneity criteria, and these tests detailed results are recorded in Table 2.

It is noted that the significance level $\alpha = 0.01$ was adopted in the research, since such a strict threshold allows us to significantly reduce the error first type probability (the null hypothesis false rejection) and thereby increase the obtained conclusion's reliability regarding the training dataset homogeneity. When analyzing the helicopter TE's gas temperature, the statistically significant effect of incorrect recognition could lead to erroneous engineering solutions and emergency operating modes, so the stricter criterion choice is justified by the need for strict safety control and the results reliability. The $\alpha = 0.01$ use provides sufficient tests of statistical power with a 1280 readings data amount, which makes the conclusions about the gas temperature time series behavior justified.

Table 1
The training dataset fragment

Number	Gas temperature normalized value
1	0.986
...	...
256	0.983
...	...
512	0.990
...	...
768	0.985
...	...
1024	0.984
...	...
1280	0.991

Table 2
The training dataset homogeneity assessing results

Criterion	Calculated value	Critical value	Decision
Fisher-Pearson	9.112	9.2	The training dataset is homogeneous since the Fisher-Pearson and Fisher-Snedecor criteria calculated values are less than the critical values.
Fisher-Snedecor	1.128	1.139	

To assess the training dataset's (see Table 1) representativeness, the k-means clustering algorithm [44, 45] was used. The original data were randomly divided in a 2:1 ratio, yielding 67 % (858 objects) for training and 33 % (422 objects) for validation. When analyzing the training part using the k-means method, the cluster number was fixed in advance at eight, which made it possible to identify eight stable groups (classes I…VIII) and, thus, confirm the training and test subdatasets similar internal structure (Figure 4). It is noted that the clustering quality can be assessed, for example, through the squared distances intracluster sum:

$$W_k = \sum_{i=1}^{k} \sum_{x_j \in C_i} \left\| x_j - \mu_i \right\|^2, \quad (25)$$

where C_i is the i-th cluster, μ_i is its center. The clusters optimal number was chosen from the "elbow" [46] on the diagram of W_k versus k.

Thus, from the total training dataset of 1280 normalized gas temperature values, 858 (67 %) were defined as the main training subdataset, and 422 (33 %) as the test subdataset.

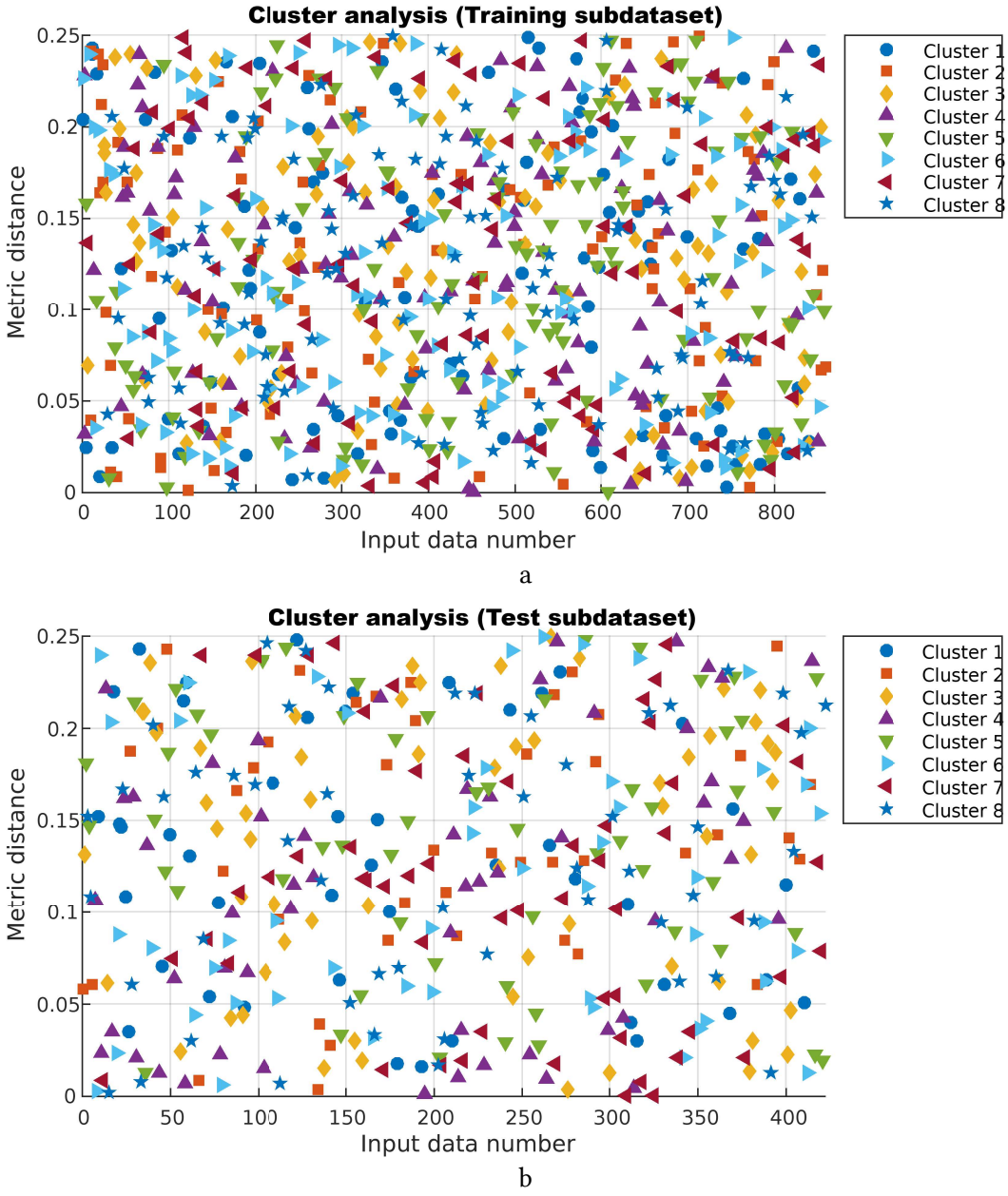

Figure 4: Cluster analysis results: (a) is the training subdataset; (b) is the test subdataset. (author's development).

4.2. The computational experiment results

The computational experiment's main result is the gas temperature in front of the compressor turbine signal resulting diagram (Figure 5), obtained using the developed model (see Figures 2 and 3).As can be seen from Figure 5, the resulting model reproduces the gas temperature dynamics reference curve's key characteristics: a smooth rise from the initial 1105 K to peak values of about 1140 K in the 120...160 seconds range, followed by a uniform decrease to about 1090 K by 310 seconds, while the fluctuation amplitude and the oscillation frequency composition practically coincide with the original experimental data. Deviations for each reading do not exceed 2...3 K, and not only the general trajectory preservation but also small peaks and troughs indicate that the

model adequately takes into account the main heat exchange and dynamic processes in the thermogasdynamic flow, which indicates high accuracy and low modeling error (Figure 6).

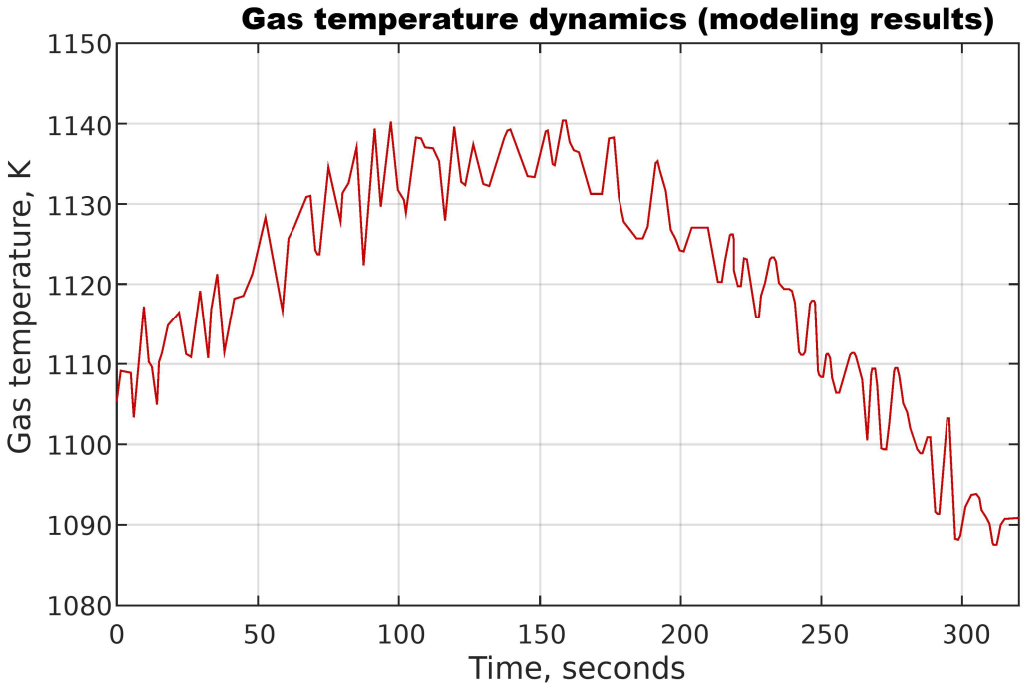

Figure 5: The gas temperature signal in front of the compressor turbine resulting diagram. (author's development).

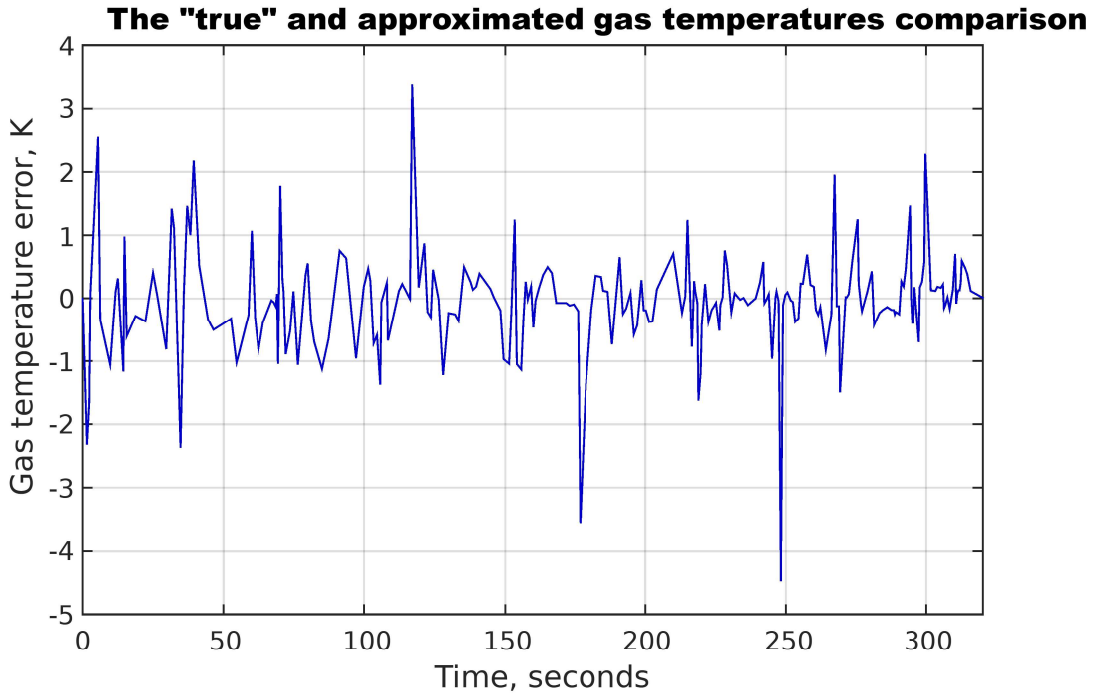

Figure 6: The gas temperature signal in front of the compressor turbine simulation error resulting diagram. (author's development).

Figure 6 shows that the approximated temperature from the “reference” gas temperature absolute deviations at most moments do not exceed ±1 K and are concentrated in a narrow range near zero, which indicates a small shear system. Single bursts up to +3...+3.5 K are observed around 120 seconds and at the experiment's end, and the maximum negative emissions up to −3...−4.5 K areapproximately at 180 and 250 seconds and are probably associated with transient phenomena and abrupt changes in heat exchange. Time intervals from 50 to 100 seconds and from 200 to 240

seconds are characterized by higher-frequency but small-scale oscillations (±1…2 K), which indicates the flow dynamic fluctuations adequately account. The average error value is close to zero, and rare large emissions are easily compensated for by the model's local refinement.

Figure 7 shows the linear term (n = 1) contribution diagram, which is the value $a_1 \cdot (T_C(t) - T_0)$ time diagram, illustrating the proportional component and its dynamics over the entire ΔT range.

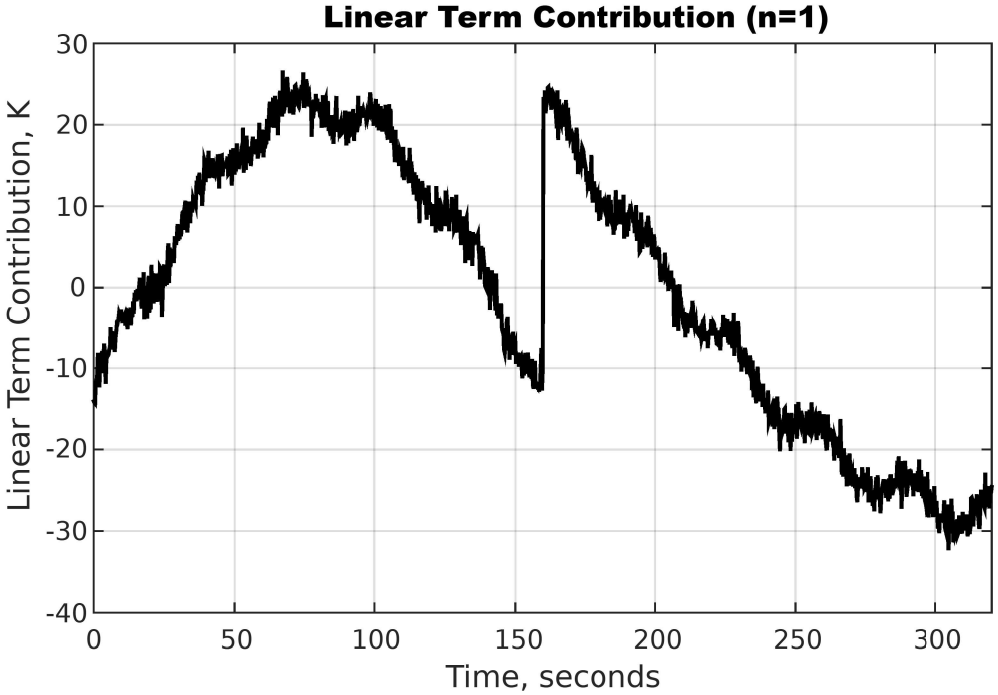

Figure 7: The linear term (n = 1) contribution diagram. (author's development).

Figure 7 shows the parameter $a_1 \cdot (T_C(t) - T_0)$ evolution, which characterizes the thermocouple output signal relative contribution dependence on the temperature increment ΔT Taylor expansion approximation linear term, experimental recording over 320 seconds. In the initial phase (0…100 seconds), a steady increase in the parameter $a_1 \cdot (T_C(t) - T_0)$ is observed from negative values to about +25 K peak, which corresponds to an increase in ΔT in the warm-up mode and the linear response predominance at small deviations from the operating point. In the 100…150 seconds region, the linear term drops sharply to negative values contribution (about −8…−12K), reflecting the transition to stronger nonlinear effects and the quadratic influence and higher orders when approaching the maximum gas temperature. In about 150 seconds, there is an instantaneous jump in the parameter $a_1 \cdot (T_C(t) - T_0)$, probably associated with the engine operating mode restructuring or switching the filtering scheme in the Simulink model, after which, in the 150…320 seconds interval, the contribution of the linear term steadily decreases to −30…−35 K, which indicates the nonlinear corrections dominance and the error accumulation at large temperature deviations from the base point. During the entire experiment, $a_1 \cdot (T_C(t) - T_0)$ (± 2…3 K) small fluctuations reflect flow pulsations and residual noise, effectively smoothed by the Kalman filter.

Figure 8 shows the parameter $a_1 \cdot (T_C(t) - T_0)$ evolution, which characterizes the thermocouple output signal relative contribution dependence on the temperature increment ΔT Taylor expansion approximation linear term, experimental recording over 320 seconds.

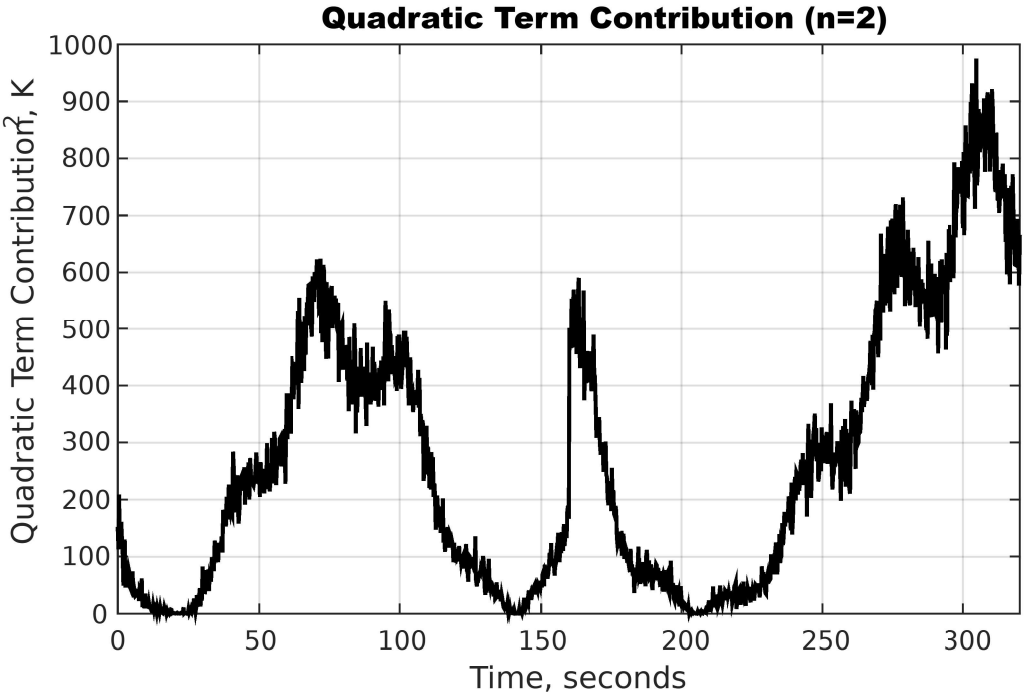

Figure 8: The quadratic term (n = 2) contribution diagram. (author's development).

Figure 8 shows that the approximation $a_2 \cdot (T_C(t) - T_0)^2$ changes quadratic term contribution in a wide range from 0 to 1000 K² depending on the operating mode: in the initial heating phase (0…50 seconds) with small temperature increments, the quadratic contribution is almost absent, then in the 50…90 seconds range it quickly increases to ~600 K², reflecting the increase in nonlinearity during the transition to moderate ΔT. Upon reaching stabilization (90…140 seconds), it again decreases to zero, to a 550 K² peak at about 160 seconds during the second short-term accelerated acceleration (probably associated with a change in the compressor load). During the final intensive run (200…300 seconds), the quadratic contribution steadily increases, reaching about 950 K² maximum before the experiment end, which indicates that with large temperature differences, it is the ΔT second power that becomes the approximation error dominant source. Small-scale fluctuations (±20 K²) correspond to residual flow pulsations and sensor noise.

Figure 9 shows the residual term $R_2(t)$ diagram, which is the residual term $R_2(t)$ estimate showing where and when the higher terms become noticeable.

In Figure 9, the second-order Taylor series $R_2(t)$ residual term, proportional to the gas temperature increment ΔT^3 cube, demonstrates a clear dependence on the heat flux dynamics: in intervals relative to the steady-state regime (approximately 0…40 seconds, 100…150 seconds, 180… 240 seconds), the R_2 value remains close to zero, which indicates the first two expansion terms dominance and the high-order nonlinear effects negligibility. During transient processes (peaks in the 50…80 seconds region, a sharp jump around 160 seconds, and the most pronounced rise in the 260…300 seconds range), the R_2 value increases to $2…3 \cdot 10^4$ K³, indicating the cubic term's significant contribution and the need to take into account higher orders with rapid temperature variability. The obtained results are fully consistent with the conclusions about the adaptive thermocouple model self-tuning, where in transient modes the model should adjust the filter and neural network parameters to compensate for the signal nonlinear and dynamic distortions.

Figure 10 shows the adaptive Kalman coefficient evolution diagram, which is the parameter K_k time diagram for the aim of analyzing the filter adjustment to changes in noise and model during helicopter flight.

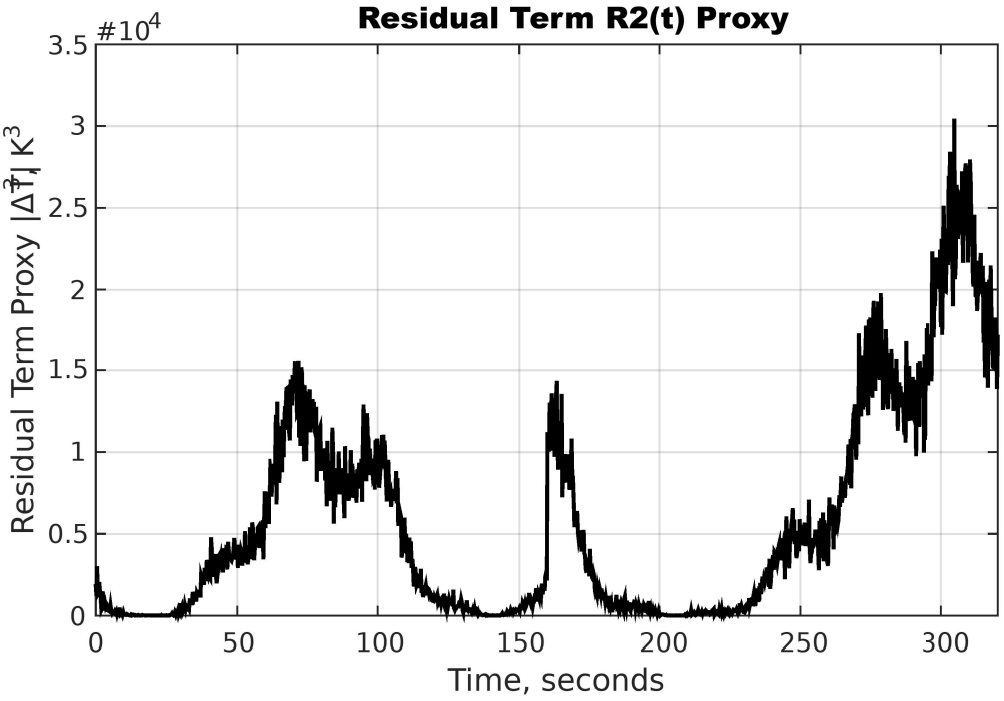

Figure 9: The second-order Taylor series residual term dynamics diagram. (author's development).

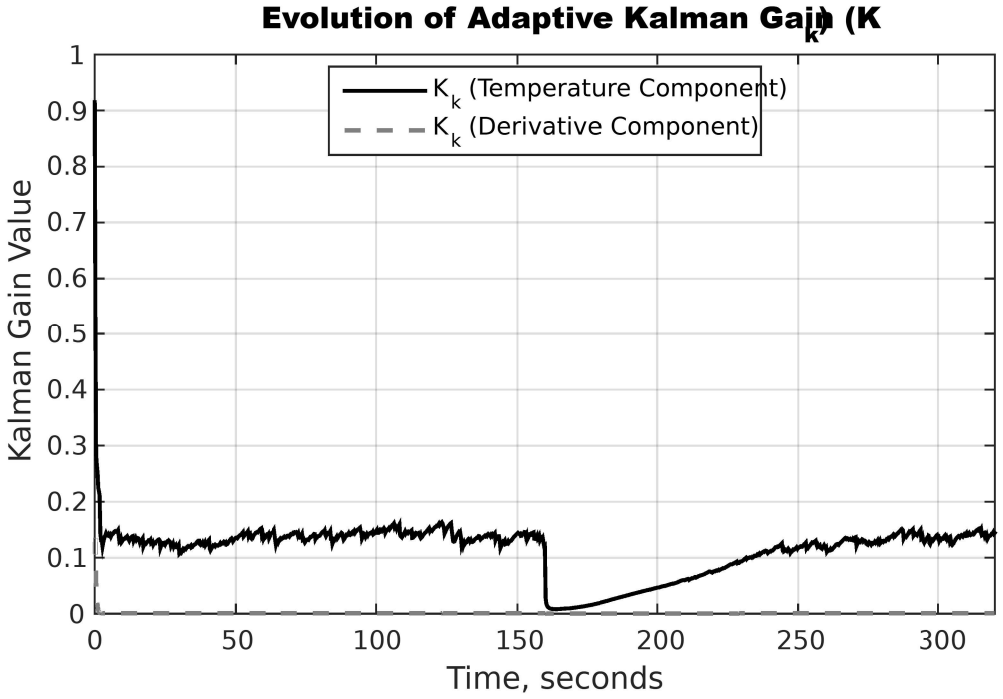

Figure 10: Adaptive Kalman coefficient evolution diagram. (author's development).

In Figure 10, the adaptive Kalman coefficients evolution, it is evident that in the initial phase (0…≈150 seconds) and with relatively smooth temperature changes, both gain components, the temperature K_k^t (solid curve) and the derivative K_k^d (dash-dotted curve), fluctuate in an approximately 0.1…0.15 narrow range, which provides a compromise between the trust in the model and the sensor signal. With a sharp transition at about 150…160 seconds, both coefficients tend to zero, which corresponds to a sharp increase in the residuals and a decrease in the noisy measurements influence on the adaptive estimate R_k according to (19).

Figure 11 shows the difference diagram in gas temperature approximations for N and $N + 1$. Figure 11 illustrates how much adding each subsequent term in the series improves (or does not) the model accuracy.

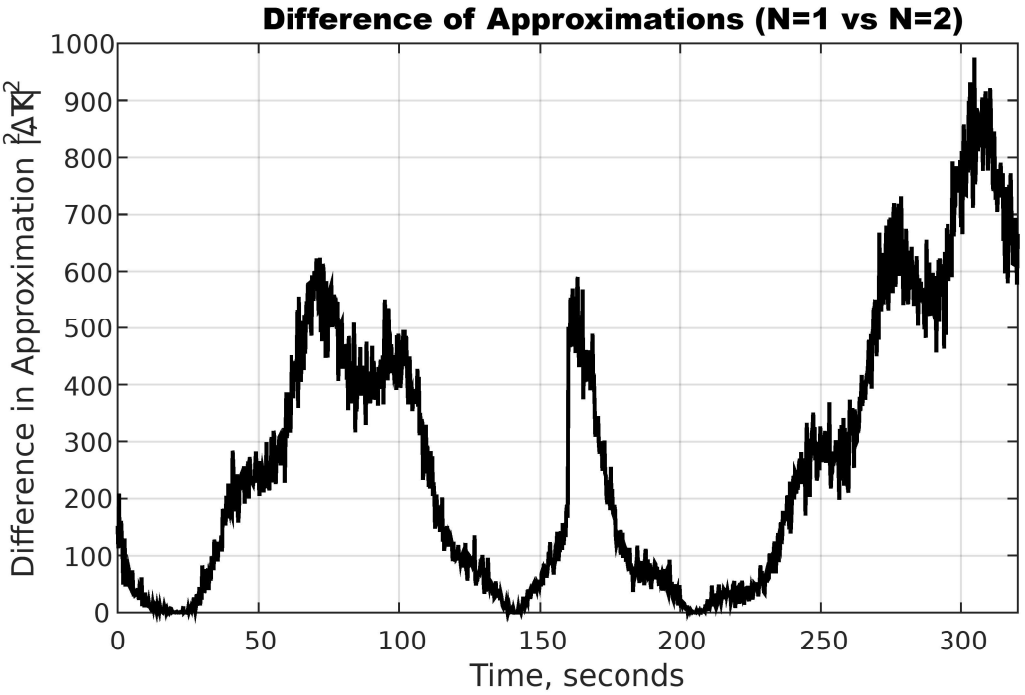

Figure 11: The difference diagram in gas temperature approximations at N and $N + 1$. (author's development).

The presented diagram of the difference in the first ($N = 1$) and second ($N = 2$) order approximation error squares (Figure 11) shows that the quadratic term inclusion in the Taylor expansion provides the greatest gain precisely at the sharp transient process moments, when ΔT reaches comparatively large values: the difference peaks up to 900…1000 K^2 fall on the rapid increase and decrease intervals in temperature (approximately 50…80 seconds, 140…155 seconds, and 260…305 seconds). At the same time, in the smooth change phases (0…30 seconds, 110…130 seconds, 180…200 seconds), the second-order advantage tends to zero (< 50 K^2). This is completely consistent with the quadratic term η_2 relative contribution estimate from (8)–(9): At $|\Delta T| > 1$ K, its influence increases sharply, and for small deviations, the linear term turns out to be sufficient for an accurate approximation.

4.3. The results obtained the quality evaluation

To evaluate the developed model with an LSTM network, an attention mechanism, and an adaptive Kalman filter (Figure 1) efficiency, used to the helicopter TE gas temperature sensor thermocouple model, two key indicators were selected: the efficiency coefficient and the quality coefficient [47, 48]. The efficiency coefficient (K_{eff}) shows how quickly and adequately the network adapts to errors in the optimization process and is calculated as the change ratio in the loss function at the current iteration to the change in the network parameters in the same iteration. The quality coefficient ($K_{quality}$) evaluates the approximation accuracy and the model convergence stability, calculated as the decrease ratio in the loss function at the current step to the previous iterations total losses. These indicators provide the LSTM network efficiency comprehensive assessment, facilitating its training characteristics objective analysis and the gas temperature sensor signals approximation accuracy. The efficiency and quality coefficients are calculated as [47, 48]:

$$K_{eff}=\frac{\left|E\left(\theta_k\right)-E\left(\theta_{k-1}\right)\right|}{\left\|\theta_k-\theta_{k-1}\right\|},\ K_{quality}=\frac{E\left(\theta_{k-1}\right)-E\left(\theta_k\right)}{E\left(\theta_0\right)-E\left(\theta_{k-1}\right)}, \quad (26)$$

where $E(\theta_0)$ is the loss function initial value, $E(\theta_k)$ is the loss function value at the current iteration, $E(\theta_{k-1})$ is the loss function value at the previous iteration, and $\|\theta_{k-1} - \theta_k\|$ is the LSTM network parameters change rate at the current iteration.

Table 3 presents a comparative analysis of the helicopter TE gas temperature in front of the compressor turbine sensor signals approximating efficiency using the developed model with an LSTM network, an attention mechanism, and an adaptive Kalman filter, as well as the recurrent neural networks and other traditional architectures adapted to similar problems [8, 9, 11, 19, 24, 35, 36, 47]: a traditional LSTM network [49, 50], a traditional GRU network [51], and a traditional RNN network [52].

Table 3

The helicopter TE gas temperature in front of the compressor turbine sensor signals approximation efficiency evaluation comparative analysis results

The recurrent neural network architecture	In the noise absence		With the white noise addition with zero mathematical expectation and σ = 0.25	
	Efficiency coefficient (K_{eff})	Quality coefficient ($K_{quality}$)	Efficiency coefficient (K_{eff})	Quality coefficient ($K_{quality}$)
Developed model with LSTM network, attention mechanism and adaptive Kalman filter	0.991	0.989	0.982	0.980
Traditional LSTM network [49, 50]	0.982	0.977	0.965	0.961
Traditional GRU network [51]	0.965	0.960	0.944	0.938
Traditional RNN network [52]	0.943	0.938	0.929	0.921

Comparative analysis (Table 3) showed that the developed model with LSTM network, attention mechanism, and adaptive Kalman filter outperforms traditional recurrent network architectures in both metrics both in the noise absence (K_{eff} = 0.991; $K_{quality}$ = 0.989) and with the white noise addition (σ = 0.25) (K_{eff} = 0.982; $K_{quality}$ = 0.980). In turn, the traditional LSTM network demonstrated slightly lower values (without noise: K_{eff} = 0.982; $K_{quality}$ = 0.977; with noise: K_{eff} = 0.965; $K_{quality}$ = 0.961), followed by the GRU network (K_{eff} = 0.965, $K_{quality}$ = 0.960 and K_{eff} = 0.944, $K_{quality}$ = 0.938) and a simple RNN network (K_{eff} = 0.943, $K_{quality}$ = 0.938 and K_{eff} = 0.929, $K_{quality}$ = 0.921). Thus, the proposed architecture provides faster adaptation to errors and more stable convergence in the helicopter TE gas temperature signals approximating.

At the developed model with an LSTM network, attention mechanism, and adaptive Kalman filter (Figure 1), effectiveness is evaluated in the next stage. The traditional metrics of accuracy,

precision, recall, and F1-score values are compared with the traditional LSTM network [49, 50], the traditional GRU network [51], and the traditional RNN network [52], which are determined according to the expressions:

$$Accuracy=\frac{TP+TN}{TP+TN+FP+FN},\ Precision=\frac{TP}{TP+FP},\ Recall=\frac{TP}{TP+FN},$$
$$F1=2\cdot\frac{Precision\cdot Recall}{Precision+Recall}, \tag{27}$$

where $TP=\left|i: y_i=1\cap \hat{y}_i=1\right|$ corresponds to the number of cases when the algorithm correctly identified the anomaly in the thermocouple signal (i.e., the real temperature deviation was detected); $TN=\left|i: y_i=0\cap \hat{y}_i=0\right|$ corresponds to the number of moments when the model correctly recognized the signal as normal (there is no anomaly and the model did not detect it); $FP=\left|i: y_i=0\cap \hat{y}_i=1\right|$ reflects the false alarms number, when in the real anomaly absence the model erroneously signaled a failure; $FN=\left|i: y_i=1\cap \hat{y}_i=0\right|$ shows the missed errors number, when the real temperature deviation remained undetected by the model.

Table 4
The helicopter TE gas temperature in front of the compressor turbine sensor signals approximation efficiency evaluation comparative analysis results

The recurrent neural network architecture	Accuracy	Precision	Recall	F1-score
Developed model with LSTM network, attention mechanism and adaptive Kalman filter	0.993	0.988	0.986	0.987
Traditional LSTM network [49, 50]	0.983	0.972	0.971	0.972
Traditional GRU network [51]	0.980	0.969	0.965	0.967
Traditional RNN network [52]	0.954	0.950	0.951	0.951

The results of the comparative analysis (Table 4) show that the proposed model based on the LSTM network with an attention mechanism and an adaptive Kalman filter provides the highest performance among the considered architectures: accuracy = 0.993, precision = 0.988, recall = 0.986, and F1-score = 0.987. The classical LSTM network is characterized by lower metric values (0.983; 0.972; 0.971; 0.972, respectively), followed by the GRU network (0.980; 0.969; 0.965; 0.967) and the simple RNN network (0.954; 0.950; 0.951; 0.951). These results demonstrate the developed model's excellent ability to accurately classify normal and abnormal thermocouple signals, minimizing both false alarms and missed real deviations.

5. Discussions

The research describes the thermocouple representation as a single-loop heat-capacity element with heat capacity C and thermal resistance R, which is formalized by differential equation (1) and its discretization by the explicit Euler scheme in formulas (2)–(3). To take into account small temperature deviations around the operating point T_0, the $f(T_C)$ dependence local approximation is introduced by expansion in a Taylor series (4)–(5), where the linear (6) and quadratic (8) terms

relative contributions are analyzed, and for order $n \geq 3$ terms, an estimate is given through η_n (10) and the residual term R_N (11) upper limit.

The proposed approach is implemented by a recurrent neural network with attention mechanisms and a Kalman filter by modifying the LSTM architecture (Figure 1), which takes the vector $\mathbf{x}_k$ (12) as input, where u_k are additional engine parameters. The hidden and cell states are updated using the classic LSTM formulas (13), after which the attention mechanism calculates the weights using formula (14) and forms an "enriched" hidden state (15), which is used to predict the gas temperature in the (16) form. The resulting estimate is then passed to the adaptive Kalman filter, which performs the prediction step according to expression (17) and correction according to formula (18), where the noise variance estimate is adapted recurrently through the residuals (19). To suppress out-of-band noise in the signal, a bandpass filter with a transfer function (20) and a convolution in the form (21) is used, and the model's final tuning is performed by minimizing the total functional with regularization according to the Kalman coefficients smoothness (22).

A computational experiment performed using the discrete thermocouple model (3) and the adaptive Kalman filter (17)–(18) prediction and correction steps showed (Figure 5) that the developed model accurately reproduces the gas temperature in front of the compressor turbine reference dynamics: a smooth increase from 1105 K to ~1140 K in the 120…160 second interval and a subsequent decrease to ~1090 K by 310 seconds, with instantaneous deviations between the real and simulated signals not exceeding 2…3 K. The simulation errors diagram (Figure 6) demonstrates that the absolute errors at most points are within ±1 K, and rare spikes up to +3…+3.5 K and −3…−4.5 K (at about 120, 180, and 250 seconds) are due to transient phenomena, indicating the numerical solution's high accuracy and low bias.

The efficiency and quality coefficients used for the LSTM network with an attention mechanism and a Kalman filter adaptability and convergence comprehensive assessment are substantiated, and then specific results of the comparative analysis are presented. Table 3 shows the K_{eff} and $K_{quality}$ values, where the developed model significantly outperforms the classical LSTM, GRU, and RNN architectures both without noise and with the white noise σ = 0.25 addition. Table 4 presents traditional classification metrics (accuracy, precision, recall, and F1 score), confirming the developed model's high accuracy (accuracy = 0.993; precision = 0.988; recall = 0.986; F1 score = 0.987).

Table 5 presents the developed model's main limitations and corresponding directions for further research.

Table 5

The helicopter TE gas temperature in front of the compressor turbine sensor signals approximation efficiency evaluation comparative analysis results

Number	Limitation	Description	Prospects for further research
1	Computational complexity	The LSTM network with attention and adaptive Kalman filter high load makes implementation on onboard computers difficult.	The lightweight architectures (ghost networks [53], weight quantization [54]) development and hardware-accelerated solutions.
2	Training dataset limitation	The representative data lack for extreme conditions (transients, extreme temperatures).	The transfer learning [55] and synthetic data generation [56] methods application. The continuous online learning organization.
3	Sensitivity to	Accuracy decreases due to the	The sensor failure detection [57]

	sensor degradation	thermocouples aging or partial failure.	and signal reconstruction mechanisms integration (hybrid neuro-filter schemes).
4	Assumption of small deviations in Taylor series	Truncating the approximation series to a low order (N = 2…3) may not take into account strong nonlinearities.	The adaptive choice approximation order research and non-regularized expansions implementation [58, 59] for extreme ΔT.
5	Instability under extreme weather conditions	The model's resistance to sudden pressure changes, vibration and humidity changes has not been sufficiently tested.	Conducting field tests [60] in various climatic zones and adapting filters to the external disturbance dynamics.

6. Conclusions

The developed dynamic thermocouple model, based on the heat balance equation discretization and supplemented by an LSTM network with an attention mechanism and an adaptive Kalman filter, demonstrated the ability to take into account in detail the main heat exchange processes in a thermogasdynamic flow. The model effectively integrates a Taylor series expansion nonlinear approximation with recurrent learning, providing the temperature deviations adequate estimate even at small ΔT and cleaning the signal from out-of-band noise before feeding it to the Kalman filter.

In the computational experiment, the reconstructed gas temperature in front of the compressor turbine signal almost completely coincided with the reference curve: an increase from 1105 to ~1140 K in 120...160 seconds and a decrease to ~1090 K by 310 seconds, while the deviations for each reading did not exceed 2...3 K and the absolute modeling error was kept within ±1 K.

To objectively evaluate the proposed architecture's adaptivity and accuracy, two integral indicators were introduced: the efficiency coefficient (K_{eff}) and the quality coefficient ($K_{quality}$), and their comparative analysis with traditional RNN architectures was performed. It is shown that the developed LSTM network with an attention mechanism and an adaptive Kalman filter outperforms classical LSTM, GRU, and RNN in both metrics both in a clean signal (K_{eff} = 0.991; $K_{quality}$ = 0.989) and when adding white noise σ = 0.25 (K_{eff} = 0.982; $K_{quality}$ = 0.980).

The results comparison based on the Accuracy, Precision, Recall and F1-score metrics confirmed the developed model leading position: the 0.993; 0.988; 0.986; 0.987 values, respectively, are significantly ahead of traditional LSTM (0.983; 0.972; 0.971; 0.972), GRU (0.980; 0.969; 0.965; 0.967) and RNN (0.954; 0.950; 0.951; 0.951).

Acknowledgements

The research was carried out with the grants support of the National Research Fund of Ukraine: “Methods and means of active and passive recognition of mines based on deep neural networks”, project registration number 273/0024 from 1/08/2024 (2023.04/0024), and "Information system development for automatic detection of misinformation sources and inauthentic behaviour of chat users", project registration number 187/0012 from 1/08/2024 (2023.04/0012).

The research was supported by the Ministry of Internal Affairs of Ukraine “Theoretical and applied aspects of the development of the aviation sphere” under Project No. 0123U104884.

Declaration on Generative AI

The authors have not employed any Generative AI tools.

References

[1] Q. Kang, H. Ji, Y. Yuan, Y. Ye, Autonomous helicopter shipboard recovery flight control design based on tau theory. Aerospace Science and Technology 159 (2025) 109956. doi: 10.1016/j.ast.2025.109956.

[2] G. Di Rito, F. Schettini, Impacts of safety on the design of light remotely-piloted helicopter flight control systems. Reliability Engineering & System Safety 149 (2016) 121–129. doi: 10.1016/j.ress.2015.12.012.

[3] J. Hu, Y. Yang, N. Hu, X. Lin, Dynamic modeling and characteristic analysis of a helicopter main reducer for tooth crack diagnosis. Measurement 247 (2025) 116823. doi: 10.1016/j.measurement.2025.116823.

[4] B. Jiang, K. Zhang, Y. Lu, Q. Miao, Fault Diagnosis and Fault-Tolerant Control of Helicopters, Reference Module in Materials Science and Materials Engineering. Elsevier, 2024. doi: 10.1016/b978-0-443-14081-5.00006-4.

[5] S. Yepifanov, O. Bondarenko, Development of Turboshaft Engine Adaptive Dynamic Model: Analysis of Estimation Errors, Transactions on Aerospace Research 2022:4 (2022) 59–71. doi: 10.2478/tar-2022-0024

[6] Y. Tan, Y. Chen, Y. Zhao, M. Liu, Z. Wang, L. Du, C. Wu, X. Xu, Recent advances in signal processing algorithms for electronic noses, Talanta 283 (2025) 127140. doi: 10.1016/j.talanta.2024.127140.

[7] T. Cao, Effective detection algorithm of electronic information and signal processing based on multi-sensor data fusion, The Egyptian Journal of Remote Sensing and Space Sciences 26:3 (2023) 519–526. doi: 10.1016/j.ejrs.2023.06.008.

[8] S. Vladov, Y. Shmelov, R. Yakovliev, Optimization of Helicopters Aircraft Engine Working Process Using Neural Networks Technologies, CEUR Workshop Proceedings 3171 (2022) 1639–1656. URL: https://ceur-ws.org/Vol-3171/paper117.pdf

[9] S. Vladov, Y. Shmelov, R. Yakovliev, Modified Helicopters Turboshaft Engines Neural Network On-board Automatic Control System Using the Adaptive Control Method, CEUR Workshop Proceedings 3309 (2022) 205–224. URL: https://ceur-ws.org/Vol-3309/paper15.pdf

[10] K. V. Santhosh, B. K. Roy, An intelligent temperature measurement technique using J type thermocouple with an optimal neural network, Sensors and Transducers, 147:12 (2012), 6–14.

[11] S. Vladov, Y. Shmelov, M. Petchenko, A Neuro-Fuzzy Expert System for the Control and Diagnostics of Helicopters Aircraft Engines Technical State, CEUR Workshop Proceedings 3013 (2021) 40–52. URL: https://ceur-ws.org/Vol-3013/20210040.pdf

[12] M. Pasieka, N. Grzesik, K. Kuźma, Simulation modeling of fuzzy logic controller for aircraft engines, International Journal of Computing 16:1 (2017) 27–33. doi: 10.47839/ijc.16.1.868

[13] J. Liu, Q. Huang, C. Ulishney, C. E. Dumitrescu, Machine learning assisted prediction of exhaust gas temperature of a heavy-duty natural gas spark ignition engine, Applied Energy 300 (2021) 117413. doi: 10.1016/j.apenergy.2021.117413.

[14] J. Seo, Y. Lim, J. Han, S. Park, Machine learning-based estimation of gaseous and particulate emissions using internally observable vehicle operating parameters, Urban Climate 52 (2023) 101734. doi: 10.1016/j.uclim.2023.101734.

[15] F. Liu, J. Yang, Q. Wang, Y. Liu, H. Wang, In-situ noncontact measurement system for nozzle throat deformation in high-temperature gas heating via laser speckle digital image correlation with wavelet smoothing of displacement field, Measurement 201 (2022) 111696. doi: 10.1016/j.measurement.2022.111696.

[16] J. Dan, W. Dang, Z. Li, P. Nan, G. Xin, K.-S. Lim, H. Ahmad, H. Yang, Compact Harmonic Vernier Sensor Based on an In-Fiber FPI with Three Reflector System for Simultaneous Gas Pressure and Temperature Measurement, Sensors, 23:8 (2023) 4142. doi: 10.3390/s23084142.

[17] C. Hu, K. Miao, M. Zhou, Y. Shen, J. Sun, Intelligent Performance Degradation Prediction of Light-Duty Gas Turbine Engine Based on Limited Data, Symmetry 17:2 (2025) 277. doi: 10.3390/sym17020277.

[18] S. Cao, H. Zuo, X. Zhao, C. Xia, Real-Time Gas Path Fault Diagnosis for Aeroengines Based on Enhanced State-Space Modeling and State Tracking, Aerospace 12:7 (2025) 588. doi: 10.3390/aerospace12070588.
[19] S. Vladov, L. Scislo, V. Sokurenko, O. Muzychuk, V. Vysotska, A. Sachenko, A. Yurko, Helicopter Turboshaft Engines' Gas Generator Rotor R.P.M. Neuro-Fuzzy On-Board Controller Development, Energies, 17:16 (2024), 4033. doi: 10.3390/en17164033.
[20] L. Shen, Y. Wang, B. Du, H. Yang, H. Fan, Remaining Useful Life Prediction of Aero-Engine Based on Improved GWO and 1DCNN, Machines 13:7 (2025) 583. doi: 10.3390/machines13070583.
[21] G. Li, L. Zhang, G. Xia, S. Li, Structural Reliability Analysis of Aero-Engine Turbine Components Based on Particle Swarm Optimization Back Propagation Neural Network, Applied Sciences 15:6 (2025) 3160. doi: 10.3390/app15063160.
[22] S. Du, W. Han, Z. Kang, F. Luo, Y. Liao, and Z. Li, A Peak-Finding Siamese Convolutional Neural Network (PF-SCNN) for Aero-Engine Hot Jet FT-IR Spectrum Classification, Aerospace 11:9 (2024) 703. doi: 10.3390/aerospace11090703.
[23] W. Gao, M. Pan, W. Zhou, F. Lu, J.-Q. Huang, Aero-Engine Modeling and Control Method with Model-Based Deep Reinforcement Learning, Aerospace 10:3 (2023) 209. doi: 10.3390/aerospace10030209.
[24] S. Vladov, Y. Shmelov, R. Yakovliev, M. Petchenko, Helicopters Turboshaft Engines Parameters Identification Using Neural Network Technologies Based on the Kalman Filter, Communications in Computer and Information Science (CCIS) book series 1980 (2023) 82–97. doi: 10.1007/978-3-031-48325-7_7
[25] X. Zhang, H. Liang, J. Feng, H. Tan, Kalman Filter Based High Precision Temperature Data Processing Method, Frontiers in Energy Research 10 (2022). doi: 10.3389/fenrg.2022.832346.
[26] Y. Wang, R.-Q. Sun, L.-F. Gou, Two-Stage Hyperelliptic Kalman Filter-Based Hybrid Fault Observer for Aeroengine Actuator under Multi-Source Uncertainty, Aerospace 11:9 (2024) 736. doi: 10.3390/aerospace11090736.
[27] H. Guo, Y. Li, C. Liu, Y. Ni, K. Tang, A Deformation Force Monitoring Method for Aero-Engine Casing Machining Based on Deep Autoregressive Network and Kalman Filter, Applied Sciences 12:14 (2022) 7014. doi: 10.3390/app12147014.
[28] C. Raikar, R. Ganguli, Denoising Signals Used in Gas Turbine Diagnostics with Ant Colony Optimized Weighted Recursive Median Filters, INAE Letters 2:3 (2017) 133–143. doi: 10.1007/s41403-017-0023-y.
[29] F. Lu, Y. Wang, J. Huang, Y. Huang, Gas Turbine Transient Performance Tracking Using Data Fusion Based on an Adaptive Particle Filter, Energies 8:12 (2015) 13911–13927. doi: 10.3390/en81212403.
[30] P. Cosenza, A.-L. Fauchille, D. Prêt, S. Hedan, A. Giraud, Statistical representative elementary area of shale inferred by micromechanics, International Journal of Engineering Science 142 (2019) 53–73. doi: 10.1016/j.ijengsci.2019.05.012.
[31] M. Komar, V. Golovko, A. Sachenko, S. Bezobrazov, Development of neural network immune detectors for computer attacks recognition and classification. In Proceedings of the 2013 IEEE 7th International Conference on Intelligent Data Acquisition and Advanced Computing Systems (IDAACS), Berlin, Germany, 2013, pp. 665–668. doi: 10.1109/IDAACS.2013.6663008.
[32] A. R. Marakhimov, K. K. Khudaybergenov, Approach to the synthesis of neural network structure during classification, International Journal of Computing 19:1 (2020) 20–26. doi: 10.47839/ijc.19.1.1689.
[33] Z. Wang, Y. Wang, X. Wang, K. Yang, Y. Zhao, A Novel Digital Twin Framework for Aeroengine Performance Diagnosis, Aerospace 10:9 (2023) 789. doi: 10.3390/aerospace10090789.
[34] T. Castiglione, D. Perrone, J. Song, L. Strafella, A. Ficarella, S. Bova, Linear model of a turboshaft aero-engine including components degradation for control-oriented applications, Energies 16:6 (2023) 2634. doi: 10.3390/en16062634.

[35] Y. Shmelov, S. Vladov, Y. Klimova, M. Kirukhina, Expert system for identification of the technical state of the aircraft engine TV3-117 in flight modes. In Proceedings of the System Analysis & Intelligent Computing : IEEE First International Conference on System Analysis & Intelligent Computing (SAIC), 08–12 October 2018, pp. 77–82. doi: 10.1109/SAIC.2018.8516864
[36] S. Vladov, A. Banasik, A. Sachenko, W. M. Kempa, V. Sokurenko, O. Muzychuk, P. Pikiewicz, A. Molga, V. Vysotska, Intelligent Method of Identifying the Nonlinear Dynamic Model for Helicopter Turboshaft Engines, Sensors 24:19 (2024) 6488. doi: 10.3390/s24196488
[37] V. Turchenko, E. Chalmers, A. Luczak, A deep convolutional auto-encoder with pooling – unpooling layers in caffe, International Journal of Computing 18:1 (2019) 8–31. doi: 10.47839/ijc.18.1.1270.
[38] Y. Ge, H.-H. Ma, L.-Q. Wang, On the smoothing explosion pressure curves using Savitzky-Golay method, Journal of Loss Prevention in the Process Industries 80 (2022) 104929. doi: 10.1016/j.jlp.2022.104929.
[39] V. Turchenko, E. Chalmers, A. Luczak, A deep convolutional auto-encoder with pooling – Unpooling layers in caffe, International Journal of Computing 18:1 (2019) 8–31. doi: 10.47839/ijc.18.1.1270.
[40] H.-Y. Kim, Statistical notes for clinical researchers: Chi-squared test and Fisher's exact test, Restorative Dentistry & Endodontics 42:2 (2017) 152. doi: 10.5395/rde.2017.42.2.152.
[41] A. Benaceur, B. Verfürth, Statistical variational data assimilation, Computer Methods in Applied Mechanics and Engineering 432 (2024) 117402. doi: 10.1016/j.cma.2024.117402.
[42] C. M. Stefanovic, A. G. Armada, X. Costa-Perez, Second Order Statistics of Fisher-Snedecor Distribution and Their Application to Burst Error Rate Analysis of Multi-Hop Communications, IEEE Open Journal of the Communications Society 3 (2022) 2407–2424. doi: 10.1109/ojcoms.2022.3224835.
[43] S. Leoshchenko, A. Oliinyk, S. Subbotin, M. Ilyashenko, T. Kolpakova, Neuroevolution methods for organizing the search for anomalies in time series, CEUR Workshop Proceedings 3392 (2023) 164–176. URL: https://ceur-ws.org/Vol-3392/paper14.pdf
[44] S. Babichev, J. Krejci, J. Bicanek, V. Lytvynenko, Gene expression sequences clustering based on the internal and external clustering quality criteria. In Proceedings of the 2017 12th International Scientific and Technical Conference on Computer Sciences and Information Technologies (CSIT), Lviv, Ukraine, 05–08 September 2017. doi: 10.1109/STC-CSIT.2017.8098744.
[45] Y. V. Bodyanskiy, O. K. Tyshchenko, A Hybrid Cascade Neuro–Fuzzy Network with Pools of Extended Neo–Fuzzy Neurons and Its Deep Learning, International Journal of Applied Mathematics and Computer Science 29:3 (2019) 477–488. doi: 10.2478/amcs-2019-0035.
[46] I. Perova, Y. Bodyanskiy, Adaptive human machine interaction approach for feature selection-extraction task in medical data mining, International Journal of Computing 17:2 (2018) 113–119. doi: 10.47839/ijc.17.2.997.
[47] S. Vladov, Y. Shmelov, R. Yakovliev, Y. Stushchankyi, Y. Havryliuk, Neural Network Method for Controlling the Helicopters Turboshaft Engines Free Turbine Speed at Flight Modes, CEUR Workshop Proceedings 3426 (2023) 89–108. URL: https://ceur-ws.org/Vol-3426/paper8.pdf
[48] C. Romesis, N. Aretakis, and K. Mathioudakis, Model-Assisted Probabilistic Neural Networks for Effective Turbofan Fault Diagnosis, Aerospace 11:11 (2024) 913. doi: 10.3390/aerospace11110913.
[49] S. Xiang, Y. Qin, J. Luo, H. Pu, and B. Tang, Multicellular LSTM-based deep learning model for aero-engine remaining useful life prediction, Reliability Engineering & System Safety 216 (2021) 107927. doi: 10.1016/j.ress.2021.107927.
[50] L. Peng, N. Wei, Applications of LSTM Model for Aeroengine Forecasting. In Proceedings of the 2020 7th International Conference on Dependable Systems and Their Applications (DSA), Xi'an, China, 28–29 November 2020. doi: 10.1109/DSA51864.2020.00030.
[51] J. Zou, P. Lin, Multichannel Attention-Based TCN-GRU Network for Remaining Useful Life Prediction of Aero-Engines, Energies 18:8 (2025) 1899. doi: 10.3390/en18081899.

[52] S. Shivansh, P. Akash Kumar, S. Sharanya, Predicting Aircraft Turbofan Engine Degradation with Recurrent Neural Networks. In Proceedings of the 2024 IEEE International Conference on Information Technology, Electronics and Intelligent Communication Systems (ICITEICS), Bangalore, India, 28–29 June 2024. doi: 10.1109/ICITEICS61368.2024.10625502.

[53] H.-J. Jin, Y.-P. Zhao, M.-N. Pan, A novel method for aero-engine time-series forecasting based on multi-resolution transformer, Expert Systems with Applications 255 (2024) 124597. doi: 10.1016/j.eswa.2024.124597.

[54] D. Sabir, M. A. Hanif, A. Hassan, S. Rehman, M. Shafique, Weight Quantization Retraining for Sparse and Compressed Spatial Domain Correlation Filters, Electronics 10:3 (2021) 351. doi: 10.3390/electronics10030351.

[55] S. Mohammadi, V. Rahmanian, S. Sattarpanah Karganroudi, M. Adda, Smart Defect Detection in Aero-Engines: Evaluating Transfer Learning with VGG19 and Data-Efficient Image Transformer Models, Machines 13:1 (2025) 49. doi: 10.3390/machines13010049.

[56] H. Schieber, K. C. Demir, C. Kleinbeck, S. H. Yang, D. Roth, Indoor Synthetic Data Generation: A Systematic Review, Computer Vision and Image Understanding 240 (2024) 103907. doi: 10.1016/j.cviu.2023.103907.

[57] S. Vladov, A. Sachenko, V. Sokurenko, O. Muzychuk, V. Vysotska, Helicopters Turboshaft Engines Neural Network Modeling under Sensor Failure, Journal of Sensor and Actuator Networks 13:5 (2024) 66. doi: 10.3390/jsan13050066.

[58] S. Pang, Q. Li, H. Feng, A hybrid onboard adaptive model for aero-engine parameter prediction, Aerospace Science and Technology 105 (2020) 105951. doi: 10.1016/j.ast.2020.105951.

[59] N. Shakhovska, V. Yakovyna, N. Kryvinska, An improved software defect prediction algorithm using self-organizing maps combined with hierarchical clustering and data preprocessing. Lecture Notes in Computer Science 12391 (2020) 414–424. doi: 10.1007/978-3-030-59003-1_27.

[60] S. Ablamskyi, O. Muzychuk, E. D'Orio, and V. Romaniuk, Taking biological samples from a person for examination in criminal proceedings: correlation between obtaining evidence and observing human rights, Revista de Direito Internacional 20:1 (2023). doi: 10.5102/rdi.v20i1.8859.